Hindawi
Geofluids
Volume 2022, Article ID 1979775, 14 pages
https://doi.org/10.1155/2022/1979775

*Research Article*

# Numerical Simulation of Gas-Solid Coupling in Pressure-Relief Gas Drainage of Short-Distance and Underprotective Steeply Inclined Coal Seam Mining

**Xinshan Peng**[1], **Zhaofeng Wang**[1,2,3,4] and **Lingling Qi**[1,2,3,4]

[1]*School of Safety Science and Engineering, Henan Polytechnic University, Jiaozuo, China*
[2]*MOE Engineering Research Center of Coal Mine Disaster Prevention and Emergency Rescue, Jiaozuo, China*
[3]*Collaborative Innovation Center of Coal Work Safety and Clean High Efficiency Utilization, Jiaozuo, China*
[4]*State Key Laboratory Cultivation Base for Gas Geology and Gas Control, China*

Correspondence should be addressed to Zhaofeng Wang; wzf3988@163.com

Received 24 April 2022; Accepted 13 June 2022; Published 13 July 2022

Academic Editor: Zhongguang Sun



The accuracy of the drainage radius plays a vital role in the gas drainage effect, and the establishment of the drainage model and numerical calculation of the model has an essential value for the accurate determination of the drainage radius. Based on the elastoplastic constitutive model of mining coal and rock mass, effective stress equation, gas content equation, gas flow continuity, and control equation established by predecessors, the gas-solid coupling model of coal-rock deformation and pressure-relief gas flow in protective layer mining was established in this paper. The numerical simulation prototype was based on the mining engineering practice of a short-distance and underprotective steep seam mining in a mine in western Henan of China. COMSOL Multiphysics coupling software was used to numerically calculate the coupling model, and the influence radius of different mining pressure-relief area and different drainage time was obtained. The results show that under the same geological conditions and mining conditions, the impact range of drilling in the pressure-relief area of the protected layer is larger than that of the nonrelief area. As the working face of the protection layer advances, the pressure-relief area of the protected layer gradually increases, the influence range of the drainage borehole increases, the drainage borehole has undergone a process of initial stress-stress concentration-stress reduction-stress recovery successively, and the strike drainage radius is larger than the inclined.

## 1. Introduction

Mineable reserves of steeply inclined coal seams account for approximately 17% of the total coal reserves. Out of these reserves, 62% are distributed in north China and the rest in south China [1]. The steeply inclined coal seam is recognized as a difficult coal seam in the mining industry. Due to its special occurrence, the steeply inclined coal seam is severely damaged by extrusion, and most of the steeply inclined coal seams are high gas or outburst coal seams. A large number of studies have shown that the mining of protective layer can release the elastic potential of coal seam, increase the permeability of coal seam, facilitate the gas flow and desorption of the protected layer, and reduce the internal energy of coal seam gas. The mining of protective layer combined with pressure-relief gas drainage is considered to be the safest and most effective regional antioutburst measure [2–5]. Protective seam mining technology involves two coal seams: the protective seam and the protected seam. Generally, the protective seam contains no potential outbursts, and the protected seam contains potential outbursts. Many studies in Chinese coalfields have focused on protective seam mining, leading to a large amount of data and achieving good effects on gas extraction [6–9].

Coal and rock mass is a multifractured porous medium composed of solid skeleton and fractured pores, whose pores and fissures are the channels for gas migration and storage [10]. In a pore-fractured coal seam, the pore system absorbs

gas and diffuses, while the fracture system seeps free gas. Under normal conditions, the diffusion and seepage are a parallel mass transfer process with the synchronous mass exchange. In the original coal body, the free gas and the adsorbed gas are in a dynamic equilibrium state, and there is constant heat exchange between them and no material transfer on the macroscopic level. The equilibrium state is mainly controlled by the environmental temperature and gas pressure of the coal body. When the coal seam is affected by mining activities, the coal-rock mass is deformed, the pore pressure changes, the original equilibrium state of gas adsorption/desorption is broken, and the coal seam gas adsorption/desorption develops in a single direction, thus forming concentration gradient and pressure gradient in the coal seam, and the resulting gas flow is called pressure-relief gas flow [11–13]. After the protective layer is mined, the overlying rock moves and deforms, the original stress balance of coal and rock is broken, and the original stress balance of the coal-rock mass is broken, which in turn causes the volumetric strain and porosity of the coal-rock mass to be changed, and the coal seam gas pressure and gas flow are changed finally [14, 15]. The change of gas pressure changes the stress state of coal-rock mass and also causes the desorption of adsorbed gas, which further changes the mechanical properties of coal [16].

This study uses the elastoplastic constitutive model of mining coal and rock mass, effective stress equation, gas content equation, gas flow continuity, and control equation established by predecessors, and the gas-solid coupling model of coal-rock deformation pressure-relief gas flow in protective layer mining was established. Furthermore, COMSOL Multiphysics coupling software was used to solve the coupling model of pressure-relief gas drainage in under-protective steep seam mining.

## 2. Gas-Solid Coupling Model

*2.1. Basic Assumption.* The research object of the gas-solid coupling model of coal-rock deformation and pressure-relief gas flow is the coupling effect between adsorption/desorption, diffusion, seepage movement of pressure-relief gas, and deformation movement of coal and rock mass. The study of gas-solid coupling law is a complicated problem, involving many disciplines such as geotechnical mechanics and seepage mechanics [17, 18]. In order to facilitate numerical solution and analysis, the following basic assumptions are put forward:

(1) The gas-solid coupling system comprises single-phase gas and solid-phase coal-rock. The stress-strain relationship conforms to the mining elastic-plastic constitutive model, and the mining coal-rock mass is regarded as a fractured pore medium

(2) The coal body cannot be hardened and is subject to correlation and regular yield loading and unloading criteria. M-c criterion is used in this paper. According to this criterion, when the pressure is not large (generally <10 MPa), the strength criterion can be expressed as follows:

$$\tau = C + \sigma \tan \psi, \tag{1}$$

where $\tau$ is shear stress (MPa); $C$ is cohesion (MPa); $\sigma$ is normal stress (MPa); and $\psi$ is internal friction angle.

(3) The coal seam contains free gas and adsorbed gas, and the relationship between gas content and pressure obeys the *Langmuir* equation [19]:

$$Q_x = \frac{abp}{(1+bp)} \frac{\rho M}{V_m}. \tag{2}$$

The free gas flow state obeys the ideal gas state equation, namely:

$$Q_y = \frac{\varphi p M}{p_0 \rho V_m} \rho, \tag{3}$$

where $Q_x$ is the mass of adsorbed gas per unit volume of coal seam, that is, the mass concentration of adsorbed gas diffusion in the coal seam (g/mL); $Q_y$ is the mass concentration of free gas (g/mL); $a$ is the limit gas adsorption capacity of coal (mL/g); $b$ is the adsorption constant ($MPa^{-1}$); $p$ is the coal seam gas pressure (MPa); $\rho$ is the coal bulk density (g/mL); $M$ is the gas molar mass ($CH_4$ is 16 g/mol); $V_m$ is the gas under standard conditions molar volume (22.4 L/mol); $\varphi$ is the coal porosity (%); and $p_0$ is the standard atmospheric pressure (0.1 MPa).

(4) The adsorption of gas is nonequilibrium adsorption

(5) The diffusion of gas in the coal seam conforms to Fick's law of diffusion, and the diffusion coefficient remains unchanged [20]:

$$m_c = -D \nabla C, \tag{4}$$

$$\text{or } m_c = -D\left(\frac{\partial C}{\partial x} i + \frac{\partial C}{\partial y} j + \frac{\partial C}{\partial z} k\right), \tag{5}$$

where $m_c$ is the diffusion flux of gas through unit area [kg/(s.m$^2$)]; $D$ is the diffusion coefficient of coal seam pore system (m$^2$/s); $C$ is the mass of adsorbed CBM contained in unit volume of coal seam, namely the diffusion mass concentration of coalbed methane in the adsorbed state in the coal seam (kg/m$^3$); $\nabla$ is the Hamiltonian operator; and $i, j, k$ is the $x, y, z$ unit vector in the coordinate directions, respectively.

(6) The seepage of gas in fractures conforms to Darcy's law, and the permeability of coal and rock mass varies with the porosity and mining stress of coal and rock mass:

$$V = -\frac{k}{\mu}(\nabla p), \tag{6}$$

$$\text{or } V = -\frac{k}{\mu}\left(\frac{\partial p}{\partial x}i + \frac{\partial p}{\partial y}j + \frac{\partial p}{\partial z}k\right), \tag{7}$$

where $V$ is the seepage velocity vector of the free gas (volume flux vector m/s); $k$ is the permeability of the coal seam fracture system ($m^2$); $\mu$ is the gas dynamic viscosity ($CH_4$ is $1.08 \times 10^{-5}$Pa · s); $p$ is the free gas in the fracture system state CBM pressure (Pa); and $i, j, k$ is the $x, y, z$ unit vector in the coordinate direction, respectively.

(7) At the same level, the original gas content and gas pressure of the coal seam are the same

(8) Gas is a positive pressure fluid, and its mass density is only related to its own pressure

According to the continuum theory, the establishment of the gas flow coupling model of mining pressure-relief needs to be based on the gas flow control equation, the gas flow continuity equation, the gas state equation of gas flow, the gas content equation of coal seam, and the coal-rock mass deformation equation [21].

### 2.2. Gas Flow Continuity Equation

*2.2.1. Continuity Equation of Diffusion Motion of Pore System.* In the pore system, take a microelement, and in time $\Delta t$, according to the principle of mass conservation, the mass of the inflowing microelement minus the sum of the outflow mass plus the generation amount of the mass source should be equal to the unit time. The mass change of the microelement, for the pore system, $q$ is a negative exchange negative mass source, kg/($m^3$.s), and then the continuous equation of the diffusion motion of the pore system is [22, 23]

$$\frac{\partial C}{\partial t} = -\nabla m_c - q. \tag{8}$$

*2.2.2. Continuity Equation of Seepage Movement in Fracture System.* Taking a microelement in the fracture system, after time $\Delta t$, the gas density $\rho$ and porosity $\varphi$ will change, which will cause the control of the fluid quality in the body to change. According to the principle of mass conservation, the mass change of the microelement includes the mass of the seepage flowing into the microelement minus the sum of the outflow mass and the input amount. The continuity equation of the seepage motion of the fracture system is

$$\frac{\partial(\rho\varphi)}{\partial t} = -\nabla \cdot (\rho V) + q. \tag{9}$$

*2.2.3. Coupling Effect between Gas Diffusion and Seepage.* The above research is carried out by dividing the flow of coal seam gas into diffusion and seepage as two open systems. The adsorption/desorption of coal seam gas and gas diffusion are regarded as a system. Gas desorption converts the adsorbed gas on the inner wall of micropores into free gas, which diffuses into the seepage system along with the pores, and the two systems complete the mass transfer through the mass exchange source. Considering gas diffusion and seepage as a semiclosed system, this system has only output, and gas diffusion and seepage will inevitably decrease concentration. Gas diffusion and seepage are controlled by concentration, influence each other, and control each other. Therefore, there is a coupling effect between gas diffusion and seepage. Since the gas adsorption and desorption only change the material form, it does not cause the change of the gas quality in the microelement. Therefore, in order to facilitate the research, analysis, and solution, the gas flow mass conservation equation is obtained by adding equations (8) and (9):

$$\frac{\partial(\rho\varphi)}{\partial t} + \frac{\partial C}{\partial t} + \nabla(\rho V + m_c) = 0. \tag{10}$$

*2.3. Adsorption Expansion Strain.* Most of the gas in the coal seam is in the adsorption state, and the size of the pore surface area in the coal mass and the strength of the attractive force between the coal molecules and between the coal molecules and the gas molecules directly affect the surface tension of the coal body and the gas adsorption capacity [24]. When the gas molecules are adsorbed by the coal, the surface tension of the coal decreases, and the volume expands and deforms. The volume expansion rate of the coal is proportional to the amount of adsorption, and the coal generates expansion stress due to the adsorption expansion under the constraint conditions [25]. Assuming that coal is an elastic body, the mechanical properties and adsorption properties are the same in all directions, the adsorption properties are not affected by external forces, the adsorption deformation of the coal skeleton contact point is in a unidirectional compression state, and because the pore pressure is also the same in all directions, the coal expands in all directions According to the relationship between the adsorption expansion stress-strain and the adsorption thermodynamic parameters, the expansion stress-strain can be expressed by the following formula [26–28]:

$$\sigma_p = \frac{2a\rho RT\left(1 - 2\mu'\right)\ln(1 + bp)}{3V_m}, \tag{11}$$

$$\varepsilon_p = \frac{2a\rho RT\ln(1 + bp)}{9V_m K}, \tag{12}$$

$$\Delta\varepsilon_p = \frac{2a\rho RT[\ln(1 + bp) - \ln(1 + bp_0)]}{9V_m K}, \tag{13}$$

where $\sigma_p$ is the adsorption expansion stress (MPa); $\mu'$ is the Poisson's ratio; $\varepsilon_p$ is the adsorption expansion strain; $\Delta\varepsilon_p$ is the adsorption expansion strain increment; $R$ is the universal gas constant, $R = 8.3143J/(\text{mol} \cdot \text{K})$; $T$ is the absolute temperature (K); and $K$ is bulk modulus. The other symbols represent the same meaning as the above.

*2.4. Relationship between Effective Stress and Pore Pressure and Adsorption Expansion Stress.* Due to adsorption expansion stress, the effective stress calculation changes. The common structural model, adsorption deformation mode, coal mass deformation mode, and coal seam stress state of gas and coal all have an impact on the connection between the two [29, 30]. The relationship between the effective stress of gas-bearing coal body, pore pressure, and adsorption expansion stress is as follows:

$$\sigma_e = \sigma - p - \sigma_p, \tag{14}$$

where $\sigma_e$ is the effective stress of gas-bearing coal body; $\sigma$ is the total stress; $p$ is the pore pressure; and $\sigma_p$ is the adsorption expansion stress.

The existence of pore pressure and adsorption expansion stress can reduce the effective stress of coal, but there are essential differences between the two [31]. The adsorption expansion stress is caused by the expansion deformation caused by the decrease of the surface energy of the coal skeleton after adsorbing the gas. The force transmission must rely on the coal skeleton, and the existence of cracks causes the reverse stress difference in the crack space due to the lack of skeleton filling [32, 33]. Even when the effective stress remains unchanged, the adsorption expansion stress still acts on the fracture surface, which leads to the closure of the fracture and affects the permeability characteristics of the fractured coal body. On the one hand, the adsorption expansion stress reduces the effective stress and promotes permeability. On the other hand, the adsorption expansion stress will lead to the closure of cracks, decrease permeability, and inhibit gas flow.

*2.5. Equations of Porosity and Permeability of Gas-Bearing Coal.* The predecessors have carried out many studies on the evolution models of porosity and permeability under adsorption expansion deformation and pore pressure. The representative models of porosity and permeability are as follows: (1) the Seidle-Huitt (S-H) model only considers the shrinkage effect of the coal matrix [34]; (2) the Palmer-Mansoori (P-M) model assumes that the deformation of the coal body is a uniaxial strain condition, which is consistent with the (SH) model, and coal permeability and porosity adopt the cubic law [35]; (3) in the Shi-Durucan (S-D) model, (SD) model and (P-M) model assume the same [36]; (4) Cui-Bustin (C-B) model deduces the change of porosity with stress and gas pressure according to the relationship between pore volume and stress [37]; (5) Robertson-Christiansen (R-C) model assumes that the coal body is under isobaric conditions, and the cubic model; on this basis, it is deduced that the permeability varies with gas pressure [38]. Among them, the most common one is the (P-M) model. The model parameters are relatively simple and easy to obtain. Under the same assumptions, the (C-B) model can also be further simplified to the (P-M) model. During the mining process of the protective layer, the movement and deformation of the overlying rock and the drainage of the pressure-relief gas from the protected layer will disturb the protected coal seam, and the original stress and pore pressure of the protected layer will change. Then the effective stress of the coal and rock mass will change. Combined with PM model and C-B model, according to the principle of effective stress of coal body, the influence of coal matrix adsorption expansion/desorption and shrinkage deformation and mining stress change, the evolution model of porosity $\varphi$ and permeability $k$ can be obtained as follows:

$$\varphi = \varphi_0 \left\{ \begin{array}{c} \exp\left\{ \left( \frac{1}{K} - \frac{1}{K_p} \right) \left[ (\sigma - p - \sigma_p) - (\sigma_0 - p_0 - \sigma_{p0}) \right] \right\} + \\ \frac{\varepsilon_p}{\varphi_0} \left( \frac{K}{M} - 1 \right) \left( \frac{p}{b+p} - \frac{p_0}{b+p_0} \right) \end{array} \right\}, \tag{15}$$

$$k = k_0 \left\{ \begin{array}{c} \exp\left\{ \left( \frac{1}{K} - \frac{1}{K_p} \right) \left[ (\sigma - p - \sigma_p) - (\sigma_0 - p_0 - \sigma_{p0}) \right] \right\} + \\ \frac{\varepsilon_p}{\varphi_0} \left( \frac{K}{M} - 1 \right) \left( \frac{p}{b+p} - \frac{p_0}{b+p_0} \right) \end{array} \right\}^3, \tag{16}$$

where $M$ is the Lame constant, $M = E(1-\mu')/(1+\mu')(1-2\mu')$; $K_p$ is the bulk modulus of pores and fissures, usually 0.6~0.8 times the bulk modulus of coal; $\varphi_0$ is the initial porosity; and $k_0$ is the initial permeability.

*2.6. Deformation Equation of Mining Coal and Rock Mass.* It is assumed that the stress state of any microelement coal-rock mass is shown in Figure 1.

For any microelement as shown in Figure 1, the stress balance equation in the three directions of $X$, $Y$, and $Z$ can be expressed as [39]

$$\left. \begin{array}{l} \frac{\partial \sigma_x}{\partial x} + \frac{\partial \tau_{xy}}{\partial y} + \frac{\partial \tau_{xz}}{\partial z} + f_x = 0 \\ \frac{\partial \sigma_y}{\partial y} + \frac{\partial \tau_{xy}}{\partial x} + \frac{\partial \tau_{yz}}{\partial z} + f_y = 0 \\ \frac{\partial \sigma_z}{\partial z} + \frac{\partial \tau_{xz}}{\partial x} + \frac{\partial \tau_{yz}}{\partial y} + f_z = 0 \end{array} \right\}. \tag{17}$$

Equation (17) can be expressed as a tensor:

$$\sigma_{ij,j} + f_i = 0. \tag{18}$$

By substituting the effective stress equation (14) into equation (18), the equilibrium differential equation for the elastic-plastic deformation of the coal-rock skeleton is obtained as

$$(\sigma - p - \sigma_p) + f_i = 0. \tag{19}$$

The geometric equation of coal and rock mass reflects the relationship between strain and displacement, and the

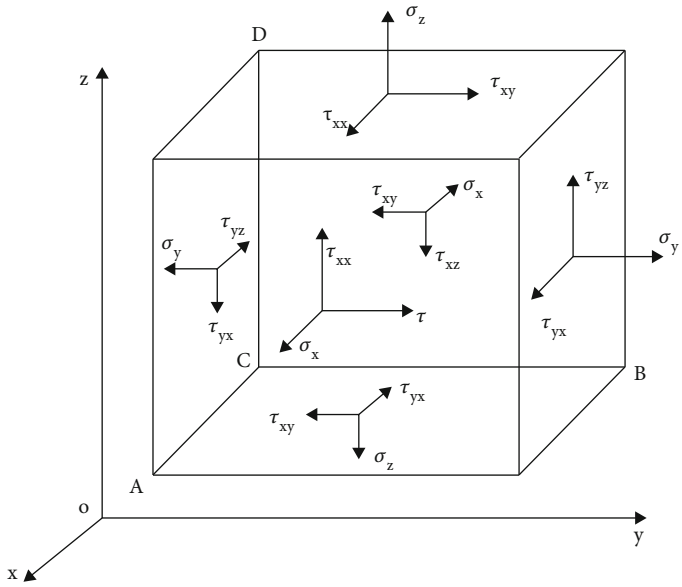


Figure 1: Stress state of the elements in coal seam.

| Lithology succession | Sequence number | Thickness (m) | Cumulative thickness (m) | Lithology description |
|---|---|---|---|---|
| | 1 | 5–14.0 | 260 | Medium-grain sandstone |
| | 2 | 16.0–44.0 | 285.4 | Sandy mudstone |
| | 3 | 3.0–11.0 | 293.8 | Medium-grain sandstone |
| | 4 | 15.0–40.0 | 324.3 | Sandy mudstone |
| | 5 | 3.0–14.0 | 330.3 | Medium-grain sandstone |
| | 6 | 7.0–18.0 | 340.8 | Sandy mudstone |
| | 7 | 3.0–12.0 | 350.8 | Quartz sandstone |
| | 8 | 10.0–40.0 | 381.6 | Quartz sandstone |
| | 9 | 2.0–6.0 | 386.0 | Argillaceous siltstone |
| | 10 | 2.0–16.0 | 392.2 | No. 2-1 coal |
| | 11 | 1.0–5.0 | 395.4 | Mudstone |
| | 12 | 2.0–12.0 | 400.4 | Sandy mudstone |
| | 13 | 3.2–11.0 | 406.2 | Siliceous mudstone, calcareous marl |
| | 14 | 0.2–2.1 | 407.3 | No. 1-8 coal |
| | 15 | 0.5–8.7 | 410.3 | Quartz sandstone |
| | 16 | 1.9–7.9 | 413.8 | Sandstone |
| | 17 | 2.0–11.0 | 422.0 | Limestone |
| | 18 | 4.0–15.0 | 432.5 | Aluminum mudstone |
| | 19 | 94.0–280 | 672.5 | Limestone |

Figure 2: Distribution of coal stratum and lithology.

tensor is in the form of

$$\varepsilon_{ij} = \frac{1}{2}\left(u_{i,j} + u_{j,i}\right), \tag{20}$$

where $\varepsilon_{ij}$ is the strain tensor and $u_{i,j}$ is the displacement tensor.

In the study of gas-solid coupling in porous media, the deformation of coal and rock mass is controlled by effective stress, and the effective stress-strain constitutive relationship of coal and rock mass satisfies the constitutive equation of generalized Hooke's law [40]:

$$\sigma_e = D_e \varepsilon_{ij}, \tag{21}$$

where $\varepsilon_{ij}$ is the coal-rock skeleton strain and $[D_e]$ is the elastic constitutive symmetry matrix of the rock. In three-dimensional coordinates, $[D_e]$ is a square matrix of order 6. For an isotropic orthotropic body, the $[D_e]$ elastic modulus $E$ and Poisson's ratio $\mu'$ can be used to represent

$$[D_e] = \frac{E}{\left(1+\mu'\right)\left(1-2\mu'\right)} \begin{bmatrix} 1-\mu' & \mu' & \mu' & 0 & 0 & 0 \\ \mu' & 1-\mu' & \mu' & 0 & 0 & 0 \\ \mu' & \mu' & 1-\mu' & 0 & 0 & 0 \\ 0 & 0 & 0 & \frac{1-2\mu'}{2} & 0 & 0 \\ 0 & 0 & 0 & 0 & \frac{1-2\mu'}{2} & 0 \\ 0 & 0 & 0 & 0 & 0 & \frac{1-2\mu'}{2} \end{bmatrix}. \tag{22}$$

## 3. Numerical Simulation

*3.1. Numerical Simulation Experimental Prototype.* In this paper, the numerical simulation is solved with the help of

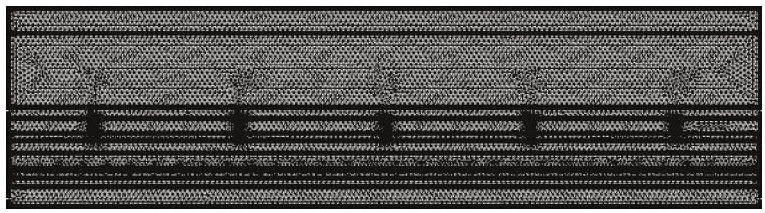

Figure 3: Strike model and meshing.

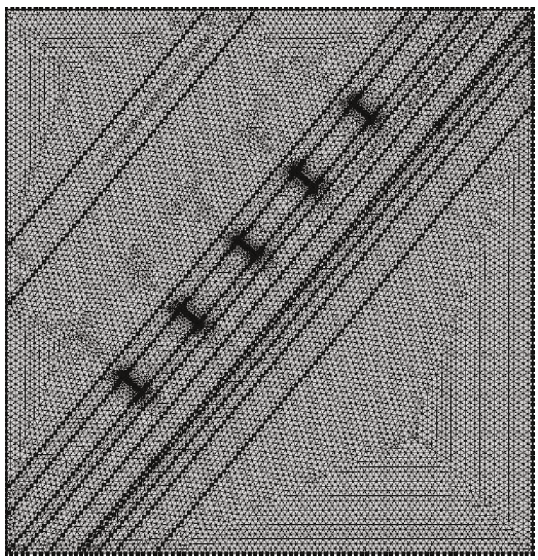

Figure 4: Inclined model and meshing.

COMSOL Multiphysics software, and the engineering and geological background is mainly based on the mining of No. 1-8 coal protected by the protected layer No. 2-1 coal seam in a mine in west Henan province, China. The average thickness of No. 1-8 coal seam is 1.1 m, and the average thickness of the vertical level is 0.71 m; the average thickness of the lead plumb of the protected layer of No. 2-1 coal seams is 6.2 m, and the average thickness of vertical level is 4.0 m; the average dip angle of coal seams is 50°, the lead plumb layer spacing of No. 2-1 coal and No. 1-8 coal is 14.0 m, and the dip distance between layers is about 9.0 m. The relative layer spacing is about 12 times the mining height of the protected layer. Its coal stratum is dominated by sandstone, mudstone, quartz sandstone, and coal seam, and the distribution of coal stratum and lithology is shown in Figure 2.

*3.2. Physical Modeling and Meshing.* The numerical simulation of protective layer working face along the inclined layout and along the strike mining establishes the numerical physical model of the inclined and strike, respectively. The length of the working face of the protection layer in strike direction is 270 m, with 20 m coal pillars at each end of the model, the total length of the model is 310 m, the height is 81.2 m, and 117,540 meshes are divided; the length of the working face in inclined direction is 75 m, the width of the model is 88.47 m, the height is 91.43 m, and 37,770 meshes are divided; the physical model and mesh division are shown in Figures 3 and 4.

*3.3. Boundary Conditions.* The average mining depth of the coal seam is 330 m, the vertical stress is 8.25 MPa, and the horizontal stress is 1.5 times of the vertical stress, which is 12.38 MPa. Only gas source exists inside the coal seam, and there is no gas flow field outside. The coal seam mining area is set as fixed as the first type of boundary conditions and fixed as atmospheric pressure 0.1 MPa, and fixed negative pressure 13 KPa is set in the borehole space.

*3.4. Initial Equilibrium of Ground Stress.* The basic parameters of the coal-rock body are assigned, and the rock mechanics parameters of the coal-rock body are shown in Table 1. These parameters can present the distribution and equilibrium state of stress in coal strata under the state of original in-situ stress.

*3.5. Gas Initial Balance.* Combined with the actual mine, the initial pore pressure, permeability, and porosity parameters of the coal seam are initially assigned, and the basic parameters of the initial state gas are shown in Table 2. The stress and gas in Table 2 are the parameters in the initial state.

*3.6. Coupling Calculation.* The protective layer working face is retrieved according to the actual control time step in the field, and the coupled calculation of gas seepage, stress, and coal-rock body deformation is performed.

## 4. Results and Analysis

*4.1. The Gas Pressure Change Rule of the Protected Layer along the Strike Direction.* Due to the large size of the strike model, if the boreholes are arranged exactly according to the actual borehole spacing in the field, the simulation results will be too dense and difficult to distinguish. In order to more intuitively observe the transport of unloading gas in the protected layer under the action of extraction, only 5 groups of drainage boreholes (boreholes are numbered from left to right as 1#~5#) are arranged in the protected layer in the strike profile; the borehole spacing is 60 m, and the borehole diameter is 100 mm. Figure 5 shows the cloud diagram of gas pressure distribution in the protected layer when 30 m, 60 m, 90 m, 120 m, 150 m, and 270 m are, respectively, mined at the working face of the protected layer.

It is evident from Figure 5 that compared with the drainage boreholes that are not subject to mining pressure-relief by the lower protective layer, the drainage influence range of the boreholes within the pressure-relief area of the

Table 1: The mechanical parameters coal and rock.

| Lithology | Volume-weight/t/m$^3$ | Poisson's ratio $\mu'$ | Internal friction angle $\varphi_/^\circ$ | Cohesion/MPa | Strength of extension $T_/$MPa | Strength of compression $\sigma$c /MPa | Elasticity modulus $E$ /GPa | Bulk modulus $K$/GPa | Shear modulus $G$/GPa |
|---|---|---|---|---|---|---|---|---|---|
| Medium-grain sandstone | 2.55 | 0.27 | 36.00 | 5.88 | 3.43 | 40.27 | 10.87 | 7.88 | 4.28 |
| Sandy mudstone | 2.53 | 0.21 | 31.50 | 5.65 | 3.70 | 34.56 | 9.23 | 5.30 | 3.81 |
| Mudstone, sandy mudstone | 2.50 | 0.20 | 31.00 | 5.03 | 3.43 | 29.54 | 7.80 | 4.33 | 3.25 |
| Quartz sandstone | 2.59 | 0.23 | 37.50 | 7.23 | 4.45 | 47.04 | 12.85 | 7.93 | 5.22 |
| Argillaceous siltstone | 2.53 | 0.20 | 38.00 | 5.43 | 3.50 | 33.64 | 8.96 | 4.98 | 3.73 |
| No. 2-1 coal | 1.46 | 0.33 | 30.00 | 0.75 | 0.55 | 4.05 | 1.95 | 1.91 | 0.73 |
| Mudstone | 2.52 | 0.20 | 30.00 | 4.19 | 2.56 | 27.43 | 7.20 | 4.00 | 3.00 |
| Siliceous mudstone, calcareous marl | 2.61 | 0.20 | 33.00 | 7.84 | 4.95 | 49.65 | 13.62 | 7.57 | 5.67 |
| No. 1-8 coal | 1.42 | 0.30 | 32.00 | 1.16 | 0.87 | 6.20 | 1.48 | 1.23 | 0.57 |
| Sandstone | 2.58 | 0.21 | 40.50 | 6.54 | 4.00 | 42.71 | 11.58 | 6.66 | 4.79 |
| Limestone | 2.55 | 0.20 | 36.50 | 6.12 | 4.22 | 35.45 | 9.48 | 5.27 | 3.95 |
| Aluminum mudstone | 2.60 | 0.26 | 33.00 | 4.87 | 2.89 | 32.82 | 8.73 | 6.06 | 3.46 |
| Limestone | 2.60 | 0.22 | 40.50 | 7.58 | 5.56 | 41.32 | 11.18 | 6.65 | 4.58 |

Table 2: Model parameters.

| Model parameter | Parameter values | Unit |
|---|---|---|
| Original gas pressure of No.2-1 coal seam, $P$ | 1.35 | MPa |
| Original gas pressure of No. 1-8 coal seam, $P$ | 0.35 | MPa |
| Original gas content of No. 2-1 coal seam, $W$ | 9.50 | m$^3$/t |
| Original gas content of No. 1-8 coal seam, $W$ | 3.42 | m$^3$/t |
| Initial permeability of coal seam, $k_0$ | 0.092 | mD |
| Diffusion coefficient of pore system in coal seam, $D$ | $3.6 \times 10^{-12}$ | m$^2$/s |
| Gas dynamic viscosity, $\mu$ | $1.08 \times 10^{-5}$ | Pa∗S |
| Gas density under standard conditions, $\rho_0$ | 0.714 | kg/m$^3$ |
| Adsorption constant, $a$ | 30.286 | m$^3$/t |
| Adsorption constant, $b$ | 0.375 | MPa$^{-1}$ |
| Molar volume of gas, $V_m$ | 0.0224 | m$^3$/mol |
| Molar mass of gas, $M$ | 0.016 | kg/mol |
| Standard atmospheric pressure, $P_0$ | 0.10 | MPa |
| Initial porosity of coal, $\varphi_0$ | 8.022 | % |

protected layer is larger, and the gas pressure around the boreholes is smaller. With the advancement of the protected layer's working face, the protected layer's unloading range gradually increases, and the influence range of the drainage borehole also increases. In addition, under the influence of mining stress, the drainage borehole undergoes the original stress-stress concentration-stress reduction-stress recovery and finally stabilizes. Figure 6 shows the curve drawn from the gas pressure of the protected seam, and the bottom of the sharp decline of the curve is the position of the extraction borehole on strike.

The law of pressure-relief gas drainage is as follows.

(1) When the lower protection layer of No. 1-8 coal is retrieved for 30 m, it can be seen from Figure 6(a) that only borehole #1 is in the pressure-relief area,

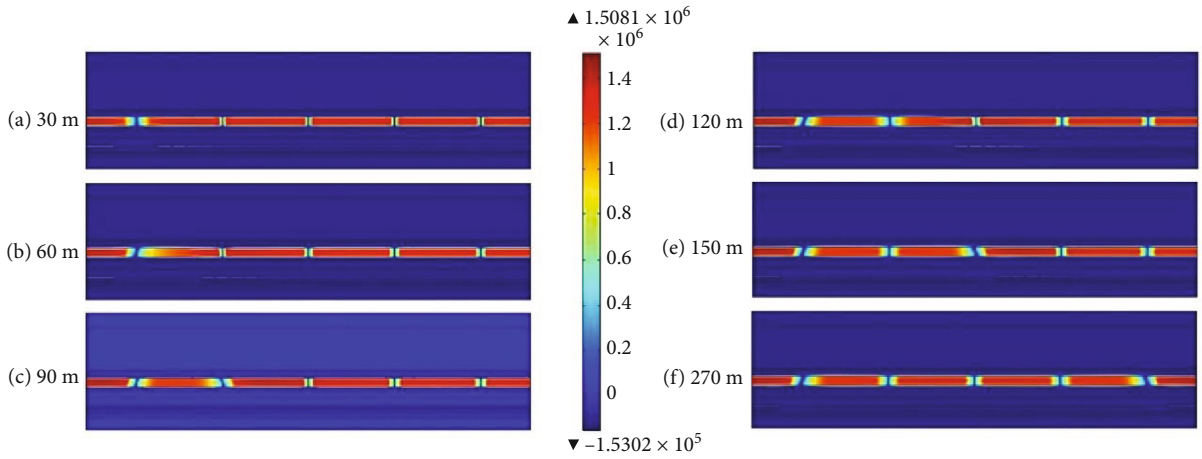


Figure 5: Scheme of gas pressure distribution of gas drainage with pressure-relief (strike).

borehole #2 is in the stress concentration area in front of the working face of the protection layer, and boreholes #3~#5 are in the original stress area; and the horizontal distance of borehole #2 from the working face of the protection layer is 45 m at this time. The effective drainage radius of borehole #1 in the pressure-relief area is 3.8 m, the effective drainage radius of borehole #2 in the stress concentration area is only 1.4 m, and the effective drainage radius of boreholes #3~5 in the original stress area is only 1.8 m

(2) From Figure 6(b), it can be seen that when the protective layer is retrieved for 60 m, only borehole #1 is still in the pressure-relief area, borehole #2 is in the area with higher stress concentration, and boreholes #3~5 are still in the original stress area. After 90 days of extraction, the effective drainage radius of borehole #1 in the pressure-relief area is 4.4 m, the effective drainage radius of borehole #2 in the pressure-relief area is reduced to 1.3 m, and the effective drainage radius of boreholes #3-5 in the original stress area is 1.9 m

(3) When the protective layer is retrieved for 90 m, borehole #1 is still in the pressure-relief area, borehole #2 also enters the pressure-relief area, borehole #3 enters the stress concentration area, and boreholes #4 and #5 are still in the original stress area, as shown in Figure 6(c). After 105 days of drainage, the effective drainage radii of boreholes 1~5# were 4.8 m, 4.9 m, 1.6 m, 2.0 m, and 2.0 m in order

(4) As the protective layer working face advances, the relief area also gradually increases. When the recovery distance increases to a certain extent, the collapsed rocks in the goaf behind the protective layer working face are gradually compacted. The coal body of the protected layer originally in the relief area is recompacted. The stress is gradually restored, at which time the permeability of the coal body of the protected layer decreases compared with the previous relief, and the drainage effect also decreases

(5) When the working face is retrieved for 150 m, it can be seen from Figures 5(e) and 6(e) that borehole #2 is exactly in the stress recovery area, and boreholes #1 and #3 are near the boundary of the pressure-relief area, borehole #4 is in the stress concentration area, and borehole #5 is in the original stress area. At this time, the effective drainage radius of boreholes 1~5# is 4.9 m, 3.5 m, 5.7 m, 2.7 m, and 3.0 m in order, and the maximum gas pressure in the stress recovery area has increased compared with the previous one, recovering to 1.27 MPa, which is slightly lower than the original gas pressure. The permeability of the corresponding areas in descending order is pressure-relief area > stress recovery area > original stress area > stress concentration area

(6) When the protective layer No. 1-8 coal is retrieved 270 m along the strike, it can be seen from Figures 5(f) and 6(f) that the mining relief range covers the area where boreholes 1#~5# are located. The pressure-relief is the most evident at the two ends of the strike open-cut eye and the stopping line, and the central part is recompacted as the stress recovery area. There is no stress concentration area directly above the mining area without leaving coal pillars in the mining area. In 200 days of drainage, the maximum effective drainage radius of the decompression area at both ends reaches 6.2 m, and the effective drainage radius of the central compaction area is only 3.9 m

*4.2. The Gas Pressure Change Rule of Protected Layer along the Inclined Direction.* The inclined model size is relatively small, in the inclined profile with a spacing of 15 m the same arrangement of 5 groups of boreholes, and borehole diameter of the same 100 mm. Considering the simulation of the working face along the inclined arrangement, along the

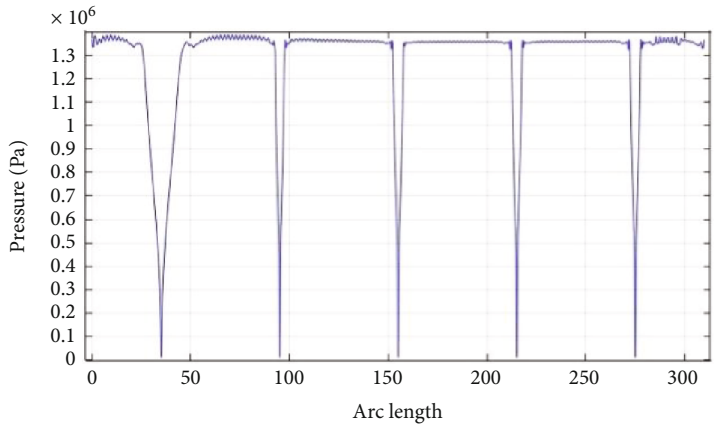


(a) 30 m

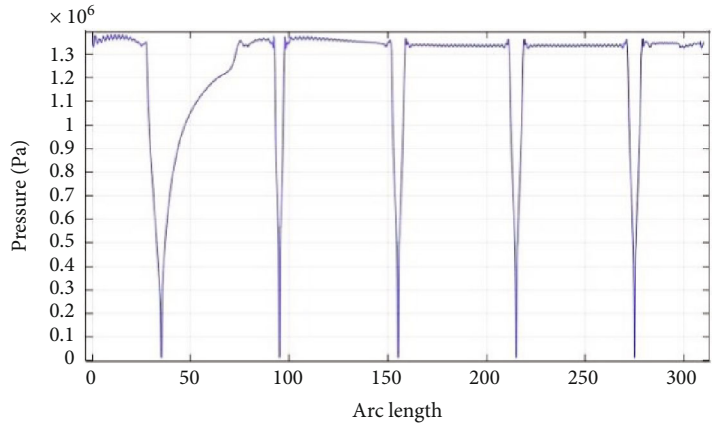


(b) 60 m

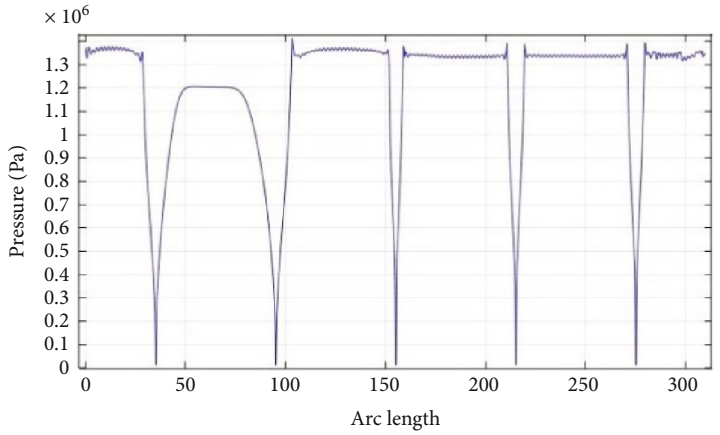


(c) 90 m

Figure 6: Continued.

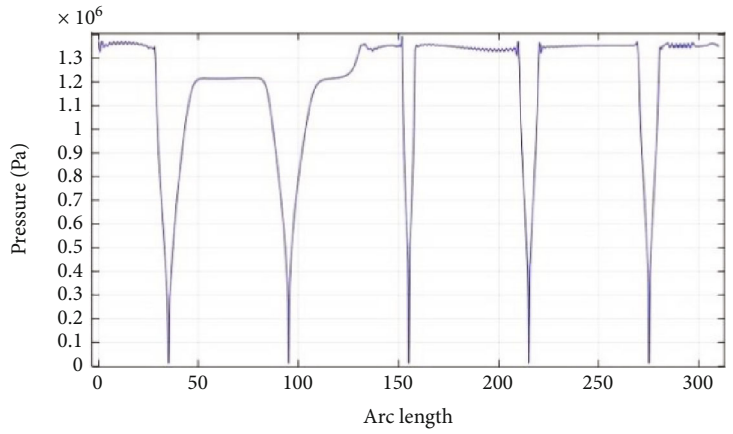


(d) 120 m

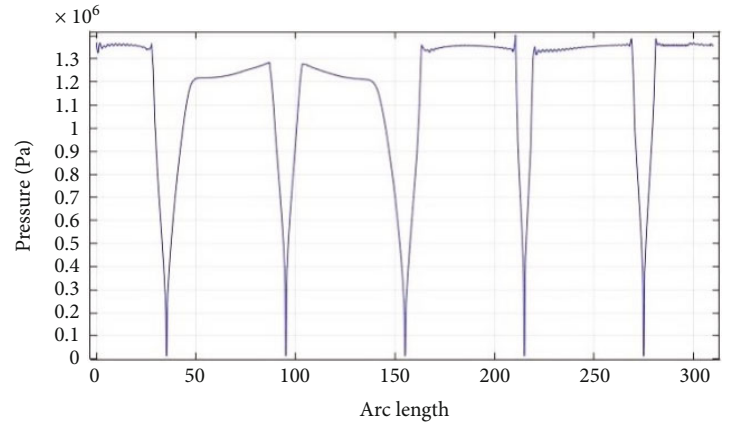


(e) 150 m

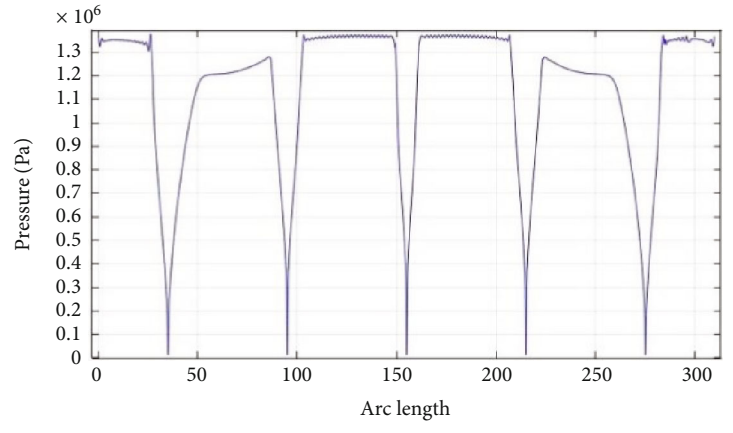


(f) 270 m

Figure 6: Curve of gas pressure distribution of gas drainage with pressure-relief (strike).

direction of recovery, inclined on the protective layer working face once finished, inclined is protected layer gas pressure distribution as shown in Figure 7.

The drainage time of 60 days, 90 days, 150 days, and 200 days was selected to protect the coal seam gas pressure along the inclined direction and plotted as a curve (Figure 8), and the bottom of the curve dropping sharply is the location of the drainage borehole on the inclined.

From Figures 7 to 8, it can be seen that the degree of pressure-relief at the inclined upper part of the tilt is significantly higher than that at the lower part, and the drainage influence range gradually increases with the increase of drainage time. The variation of the pressure-relief drainage radius with drainage time is shown in Table 3, and a logarithmic relationship was found when the two were fitted (as shown in Figure 9).

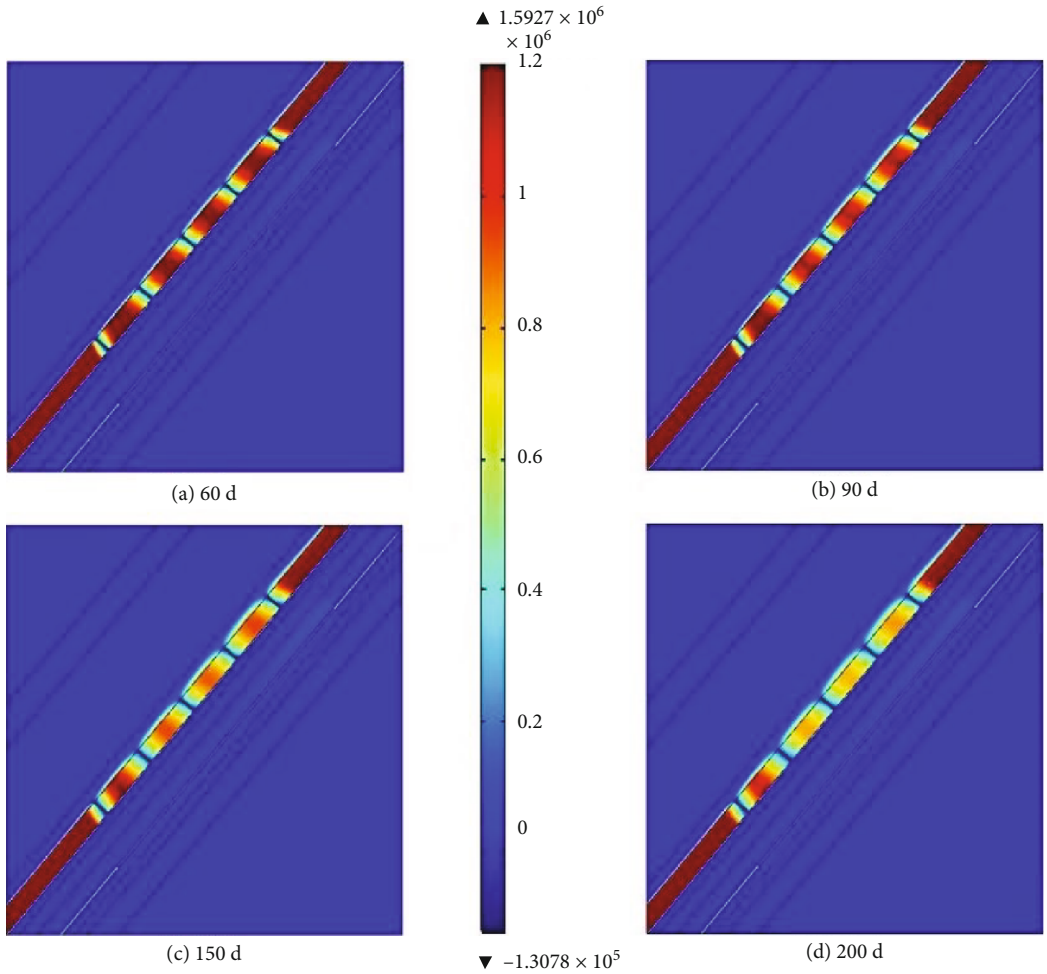


Figure 7: Scheme of gas pressure distribution of gas drainage with pressure-relief (inclined).

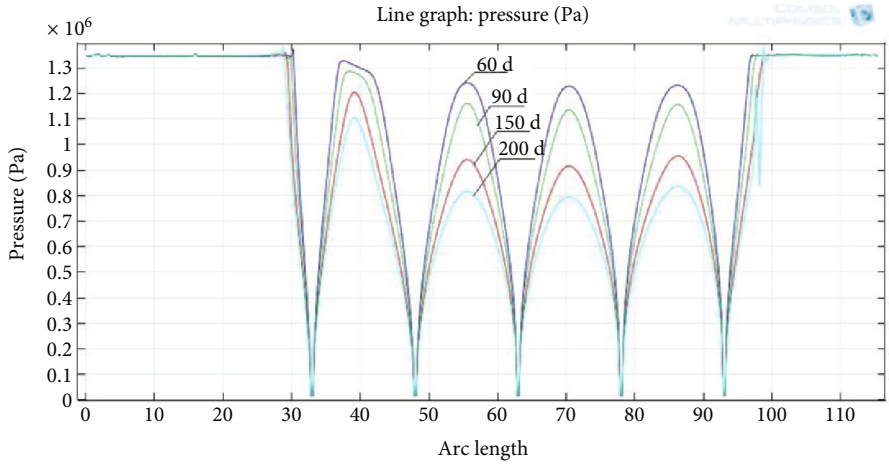


Figure 8: Curve of gas pressure distribution of gas drainage with pressure-relief (inclined).

When the protective layer workings are mined over, the fissures around the protective layer drainage area can be maintained for a long time, which is the full pressure-relief area and can be used as the main action area for gas drainage. After the overlying rock layer is moved and stabilized, a larger stress recovery area will appear in the middle of the protected layer. The lower part of the inclined is less depressurized than the upper part, and the spacing of drainage boreholes in this area should be shortened appropriately. In addition, from the comparison of inclined and strike, the

Table 3: Radius of gas drainage with pressure-relief (strike).

| Gas drainage time (day) | Radius of gas drainage with pressure-relief (m) |
|---|---|
| 60 | 2.3 |
| 75 | 2.6 |
| 90 | 3.0 |
| 105 | 3.1 |
| 120 | 3.2 |
| 135 | 3.7 |
| 150 | 4.0 |
| 200 | 4.9 |

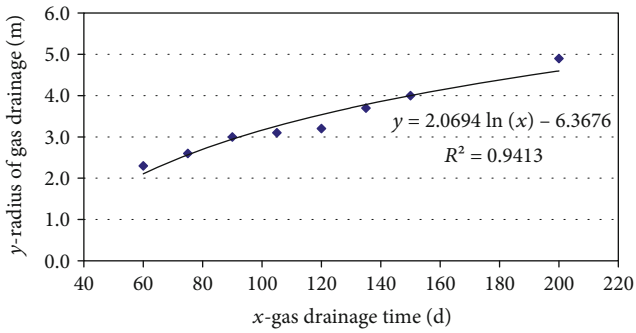


Figure 9: Variation of gas drainage radius of pressure-relief with time.

inclined drainage radius is smaller than the strike. When arranging drainage boreholes, the spacing between boreholes in the inclined direction should be smaller than that in the strike direction. Intensive drilling should be carried out in the protection and expansion boundary areas, especially in the inclined lower boundary areas.

To sum up, in the process of protected seam mining, the coal body of the protected seam all undergoes the process of "stress concentration→pressure-relief→stress recovery," and the space and time for sufficient pressure-relief should be grasped to drain the pressure-relief gas from the protected seam efficiently.

## 5. Conclusions

(1) On the one hand, the adsorption expansion stress reduces the effective stress and promotes the permeability. On the other hand, the adsorption expansion stress will lead to the closure of cracks, decrease the permeability, and inhibit the flow of gas

(2) Compared with the drainage boreholes that are not affected by the mining pressure-relief effect of the protective layer, the drainage boreholes within the pressure-relief area of the protective layer have a larger influence, and the gas pressure around the boreholes is smaller. With the advance of the working face of the protective layer, the pressure-relief area of the protected layer gradually increases, and the influence range of the drainage borehole also increases. In addition, under the influence of mining stress, the drainage borehole has undergone a process of initial stress-stress concentration-stress reduction-stress recovery

(3) When coal mining is completed, the pressure-relief is most obvious at both ends of the strike opening hole and stop-mining line, and the central recompaction is the stress recovery area. Under the condition that no coal pillar is left in the goaf, there is no stress concentration area directly above the goaf. After 200 days of drainage, the maximum effective drainage radius of the pressure-relief area at both ends is 6.2 m, and the effective drainage radius of the central compaction area is only 3.9 m. The degree of pressure-relief in the inclined upper part is higher than in the lower part. With the increase of drainage time, the influence range of drainage gradually increases, and the relationship between drainage radius and drainage time is logarithmic. The maximum effective drainage radius of the inclined pressure-relief area is 4.9 m at 200 days of drainage

(4) The fissures around the goaf of the protective layer can be maintained for a long time. In order to fully relieve the pressure, it can be used as the main area for gas drainage, and the middle of the protected layer is the stress recovery area. The pressure-relief degree of the inclined lower part is smaller than that of the upper part. From the comparison between the inclined and strike, the radius of the inclined extraction is smaller than that of the strike. When the boreholes are arranged, the spacing of the boreholes in the inclined direction should be smaller than that in the strike direction. Intensive boreholes should be carried out in the protected and extended boundary areas, especially in the inclined lower boundary areas

## Data Availability

The test data used to support the findings of this study are included within the article. Readers can obtain data supporting the research results from the test data table in the paper.

## Conflicts of Interest

The authors declare that they have no conflicts of interest.

## Acknowledgments

This research was supported by the National Natural Science Foundation of China (Nos. 52074107 and 51704100); the Doctoral Fund of Henan Polytechnic University (No. B2016-004); the Postdoctoral Research Foundation of Henan Province (Third-Class Financial Support & First-Class Financial Support); the Henan Provincial Key Laboratory of Gas Geology and Gas Control-Open Project of the State Key Laboratory Cultivation Base jointly built by the

province and the ministry (No. WS2018B13); the Fundamental and Frontier Technology Research Project of Henan Province (No. 162300410038); and the Key Scientific Research Project of Higher Education Institutions of Henan Provincial Department of Education (No. 15A440007).

## References

[1] H. S. Tu, S. H. Tu, Y. Yuan, F. T. Wang, and Q. S. Bai, "Present situation of fully mechanized mining technology for steeply inclined coal seams in China," *Arabian Journal of Geosciences*, vol. 8, no. 7, pp. 4485–4494, 2015.

[2] H. F. Wang, Y. P. Cheng, and L. Yuan, "Gas outburst disasters and the mining technology of key protective seam in coal seam group in the Huainan coalfield," *Natural Hazards*, vol. 67, no. 2, pp. 763–782, 2013.

[3] H. B. Liu, H. Liu, and Y. P. Cheng, "The elimination of coal and gas outburst disasters by ultrathin protective seam drilling combined with stress-relief gas drainage in Xinggong coalfield," *Journal of Natural Gas Science and Engineering*, vol. 21, pp. 837–844, 2014.

[4] L. Wang, Z. Lu, D. P. Chena et al., "Safe strategy for coal and gas outburst prevention in deep-and-thick coal seams using a soft rock protective layer mining," *Safety Science*, vol. 129, p. 104800, 2020.

[5] H. B. Liu and Y. P. Cheng, "The elimination of coal and gas outburst disasters by long distance lower protective seam mining combined with stress-relief gas extraction in the Huaibei coal mine area," *Journal of Natural Gas Science and Engineering*, vol. 27, pp. 346–353, 2015.

[6] L. Yuan, "Research on gas drainage technology for seam group with complicated and difficult conditions," *Coal Science and Technology*, vol. 31, no. 11, pp. 1–4, 2004.

[7] Y. P. Cheng, Q. X. Yu, and L. Yuan, "Experimental research of safe and high-efficient exploitation of coal and pressure relief gas in long distance," *Journal of China University of Mining and Technology*, vol. 33, pp. 132–136, 2004.

[8] M. Tu, N. B. Huang, and B. A. Liu, "Research on pressure-relief effect of overlying coal rock body using far distance lower protective seam exploitation method," *Journal of Mining & Safety Engineering*, vol. 24, no. 4, pp. 418–421, 2007.

[9] L. Wang, Y. P. Cheng, F. R. Li, H. F. Wang, and H. B. Liu, "Fracture evolution and pressure relief gas drainage from distant protected coal seams under an extremely thick key stratum," *Journal of China University of Mining and Technology*, vol. 18, no. 2, pp. 182–186, 2008.

[10] S. B. Hu, E. Y. Wang, and X. F. Liu, "Effective stress of gas-bearing coal and its dual pore damage constitutive model," *International Journal of Damage Mechanics*, vol. 25, no. 4, pp. 468–490, 2016.

[11] W. Li, Y. Cheng, P. K. Guo, F. H. An, and M. Y. Chen, "The evolution of permeability and gas composition during remote protective longwall mining and stress-relief gas drainage: a case study of the underground Haishiwan Coal Mine," *Geosciences Journal*, vol. 18, no. 4, pp. 427–437, 2014.

[12] W. Yang, B. Q. Lin, Y. A. Qu et al., "Mechanism of strata deformation under protective seam and its application for relieved methane control," *International Journal of Coal Geology*, vol. 85, no. 3-4, pp. 300–306, 2011.

[13] W. Yang, B. Q. Lin, Y. A. Qu et al., "Stress evolution with time and space during mining of a coal seam," *International Journal of Rock Mechanics and Mining Sciences*, vol. 48, no. 7, pp. 1145–1152, 2011.

[14] H. Y. Liu, Y. P. Cheng, H. D. Chen, J. H. Mou, and S. L. Kong, "Characteristics of mining gas channel expansion in the remote overlying strata and its control of gas flow," *International Journal of Mining Science and Technology*, vol. 23, no. 4, pp. 481–487, 2013.

[15] Y. Y. Zhao, D. X. Cui, J. S. Liu, M. Y. Wei, and Y. K. Liu, "Evolution of coal permeability under constant effective stresses: direct measurements and numerical modeling," *Energy & Fuels*, vol. 35, no. 19, pp. 15489–15501, 2021.

[16] A. Liu, S. M. Liu, P. Liu, and S. Harpalani, "The role of sorption-induced coal matrix shrinkage on permeability and stress evolutions under replicated in situ condition for CBM reservoirs," *Fuel*, vol. 294, p. 120530, 2021.

[17] A. Liu and S. M. Liu, "A fully-coupled water-vapor flow and rock deformation/damage model for shale and coal: its application for mine stability evaluation," *International Journal of Rock Mechanics and Mining Sciences*, vol. 146, p. 104880, 2021.

[18] C. P. Xin, F. Du, K. Wang, C. Xu, S. G. Huang, and J. T. Shen, "Damage evolution analysis and gas-solid coupling model for coal containing gas," *Geomechanics and Geophysics for Geo-energy and Geo-resources*, vol. 7, no. 1, pp. 1–15, 2021.

[19] K. Sing and D. Everett, "Reporting physisorption data for gas/solid systems with special reference to the determination of surface area and porosity (provisional)," *Pure and Applied Chemistry*, vol. 54, no. 11, pp. 2201–2218, 1982.

[20] Y. Qiluan and W. Youan, "Theory of methane diffusion from coal cuttings and its application," *Mei T'an Hsueh Pao; (China)*, vol. 3, 1986.

[21] G. Z. Yin, M. H. Li, J. G. Wang, J. Xu, and W. P. Li, "Mechanical behavior and permeability evolution of gas infiltrated coals during protective layer mining," *International Journal of Rock Mechanics and Mining Sciences*, vol. 80, pp. 292–301, 2015.

[22] G. D. Wang, T. Ren, Q. X. Qi, J. Lin, Q. Q. Liu, and J. Zhang, "Determining the diffusion coefficient of gas diffusion in coal: development of numerical solution," *Fuel*, vol. 196, pp. 47–58, 2017.

[23] T. H. Yang, T. Xu, H. Y. Liu, C. A. Tang, B. M. Shi, and Q. X. Yu, "Stress–damage–flow coupling model and its application to pressure relief coal bed methane in deep coal seam," *International Journal of Coal Geology*, vol. 86, no. 4, pp. 357–366, 2011.

[24] L. Zhang, T. Ren, N. Aziz, and S. Tu, "Coal sorption characteristics and coal surface tension," *Gas and Coal Technology*, vol. 8, no. 3, pp. 336–352, 2014.

[25] J. Q. Kang, D. Elsworth, X. H. Fu, S. Liang, and H. Chen, "Contribution of thermal expansion on gas adsorption to coal sorption-induced swelling," *Chemical Engineering Journal*, vol. 432, p. 134427, 2022.

[26] J. Kong, B. Q. Lin, C. J. Zhu, T. Liu, and X. G. Kong, "Impact of dynamic elastic modulus on coal permeability: modeling and analysis," *Geofluids*, vol. 2022, 11 pages, 2022.

[27] A. P. He, H. Fu, B. J. Huo, and C. J. Fu, "Permeability enhancement of coal seam by lower protective layer mining for gas outburst prevention," *Shock and Vibration*, vol. 2020, Article ID 8878873, 12 pages, 2020.

[28] J. X. Dang, M. Tu, X. Y. Zhang, and Q. W. Bu, "Analysis of the influence of upper protective layer mining on the effect of pressure relief and protection of coal and rock masses between the lower overburden layers," *Advances in Civil Engineering*, vol. 2021, Article ID 8682156, 6 pages, 2021.

[29] C. Yao, B. Li, Z. Gao et al., "Impact of sorption-induced strain and effective stress on the evolution of coal permeability under different boundary conditions," *Energy & Fuels*, vol. 35, no. 18, pp. 14580–14596, 2021.

[30] J. Liu, Z. Chen, D. Elsworth, X. Miao, and X. Mao, "Evolution of coal permeability from stress-controlled to displacement-controlled swelling conditions," *Fuel*, vol. 90, no. 10, pp. 2987–2997, 2011.

[31] B. Li, K. Yang, C. Ren, J. Li, and J. Xu, "An adsorption-permeability model of coal with slippage effect under stress and temperature coupling condition," *Journal of Natural Gas Science and Engineering*, vol. 71, p. 102983, 2019.

[32] S. B. Hu, E. Y. Wang, X. Li, and B. Bai, "Effects of gas adsorption on mechanical properties and erosion mechanism of coal," *Journal of Natural Gas Science and Engineering*, vol. 30, pp. 531–538, 2016.

[33] Y. Yu, Z. Meng, C. Gao, Y. Lu, and J. Li, "Experimental investigation of pore pressure effect on coal sample permeability under different temperatures," *Natural Resources Research*, vol. 31, no. 3, pp. 1585–1599, 2022.

[34] J. R. Seidle and L. G. Huitt, *Experimental Measurement of Coal Matrix Shrinkage Due to Gas Desorption and Implications for Cleat Permeability Increases*, In International meeting on petroleum Engineering, One Petro, 1995.

[35] I. Palmer and J. Mansoori, *How Permeability Depends on Stress and Pore Pressure in Coalbeds: A New Model*, In SPE annual technical conference and exhibition, One Petro, 1996.

[36] J. Q. Shi and S. Durucan, "Drawdown induced changes in permeability of coalbeds: a new interpretation of the reservoir response to primary recovery," *Transport in Porous Media*, vol. 56, no. 1, pp. 1–16, 2004.

[37] X. Cui and R. M. Bustin, "Volumetric strain associated with methane desorption and its impact on coalbed gas production from deep coal seams," *AAPG Bulletin*, vol. 89, no. 9, pp. 1181–1202, 2005.

[38] E. P. Robertson and R. L. Christiansen, "A permeability model for coal and other fractured, sorptive-elastic media," *SPE Journal*, vol. 13, no. 3, pp. 314–324, 2008.

[39] Y. P. Cheng, Q. Q. Liu, and T. Ren, *Coal mechanics*, Springer, Singapore, 2021.

[40] J. Li, B. Li, Q. Cheng, and Z. Gao, "Evolution of anisotropic coal permeability under the effect of heterogeneous deformation of fractures," *Natural Resources Research*, vol. 30, no. 5, pp. 3623–3642, 2021.